Check for updates

# Phosphorous-functionalized PAMAM dendrimers supported on mesoporous silica for Zr(IV) and Hf(IV) separation

Wei Qin, [ID] [a] Kaixuan Xu,[a] Junwei Wang,*[a] Xiaofeng Cui,[a] Jianli Zhang[b] and Yaqing Weng[c]

To overcome the urgency of zirconium and hafnium separation, a novel mesoporous silica sorbent (PS-G1.0-MSNs) modified with phosphorous-functionalized G1.0 PAMAM dendrimers was prepared. The adsorption and separation behaviors of PS-G1.0-MSNs adsorbent on Zr(IV) and Hf(IV) were perfromed as a function of acidity, contact time, temperature, and ion concentrations by batch sorption methods. The maximum adsorption capacities for Zr(IV) and Hf(IV) were 25.7 mg g$^{-1}$ and 5.36 mg g$^{-1}$ under optimal experimental conditions, respectively, and the separation factor $\beta_{Hf/Zr} = 2.0 > 1$ demonstrated that the prepared sorbent had preferential selectivity for Hf(IV) in rich Zr(IV) solution. Moreover, kinetic data indicated that the sorption process on Zr(IV) and Hf(IV) achieved equilibrium within 120 min, and followed the pseudo-first-order model with a rate-determining step. The adsorption amount increased as temperature raised from 283 K to 303 K and the isothermal data plotted with the Langmuir model was better than the Freundlich model with monolayer behavior. Thermodynamic data analysis indicated that the sorption process was spontaneous and endothermic. Furthermore, XPS analysis revealed that the metal ion adsorption was mainly induced by the chemical coordination of Zr(IV) and Hf(IV) ions with N, O, P atoms of amide and phosphate groups. The present work provides good guidelines on the design of high efficient sorbent for the separation of Hf(IV) from Zr(IV) solutions.

## 1. Introduction

Zirconium and hafnium coexist commonly in nature and they have similar great chemical properties. However, the applications of zirconium and hafnium are completely different in the nuclear industry. Zirconium is used as a cladding material due to its low thermal neutron capture, whereas hafnium is employed as a controlling material due to its higher neutron adsorption cross-section.[1] The hafnium content should be less than 100 ppm for application in the nuclear industry, as well as other applications, so zirconium and hafnium must be separated before using.[2] The amount of hafnium in zirconium is about 1–3% in natural sources if the hafnium can be extracted from zirconium-rich solution preferentially, which is of important practical significance for simplifying the separation process and reducing the amount of organic phase. Many extractants such as D2EHPA,[3] PC-88A,[4] BEAP,[5] Cyanex,[6] alamine,[7] and synergistic extractants TOA-Cyanes921,[8] TOPO-

Cyanes272 (ref. 9) and LIX63-PC88A[10] preferentially extract zirconium instead of hafnium. Industrially, about two-thirds of nuclear-grade hafnium and zirconium have been extracted by MIBK separation technology,[11] moreover, the MIBK extractant can preferentially extract hafnium from zirconium solution and the separation factor of hafnium to zirconium is up to 10. However, it is difficult to widely apply MIBK technology due to the high solvent consumption, volatilization, risk of explosion, high solubility of the extractant in water, and large investment in environmental pollution control.[12] The development of a highly efficient method using specific ion recognition technology to separate hafnium from zirconium instead of a traditional MIBK process is needed urgently.

Many methods have been investigated for Zr(IV)/Hf(IV) separation; the adsorption technology using polymer sorbents is one method that has been used to separate metal ions because of the minimal organic solvent utilization, less waste accumulation, reusability, and simple operation.[13,14] Hence, as an alternative separation method, the adsorption method used for the separation of zirconium and hafnium is desirable.[15] The selectivity and adsorption amount mainly lie in the functional groups of chelating resins for the adsorption approach. Among the various extractants, polyamidoamine dendrimers (PAMAM) have caused widespread concern about metal ion adsorption due to their easily functionalized groups of –NH$_2$ and esters on

[a]*Anhui Province Key Laboratory of Optoelectronic and Magnetism Functional Materials, Anqing Normal University, Anqing 246011, China. E-mail: wangjunweilotus@163.com; Tel: +86-556-5708017*

[b]*State Key Laboratory of High-efficiency Utilization of Coal and Green Chemical Engineering, Ningxia University, Yinchuan 750021, China*

[c]*Jiangxi Academy of Sciences, Nanchang 330012, China*

terminal surfaces.[16–18] According to the report that the PAMAM dendrimer is a good chelating agent with a high capacity for the removal of many metal ions, such as mercury, lead, copper, uranium, and so on, from aqueous solution.[19–21] However, PAMAM dendrimers are easily soluble in water, which makes them hard to reuse and widespread using. Therefore, immobilizing PAMAM dendrimers on supports such as silica gel,[22–26] titania,[27] chitosan,[28] graphene oxide[29] and CNT[30,31] to prepare solid extractants is an alternative method. Among these supports, mesoporous silica is an ideal inorganic solid support due to its well-modified surface properties, mechanical stability, rapid adsorption kinetics and chemical stability, and it has been widely used as a carrier modified with $-NH_2$, $-SH$, $-SO_3H$, and $-PO_3H_2$ in previous research to enhance the adsorption capacity on metal ions.[32–34]

In the present study, a phosphorous-modified G1.0 PAMAM dendrimer was covalently immobilized on mesoporous silica to prepare a sorbent (PS-G1.0-MSNs for short) for the separation of Zr(IV) and Hf(IV). Adsorption and separation properties of Zr(IV) and Hf(IV) on this sorbent were studied by batch experimental parameters, such as solution acidity, contact time, temperature, and concentrations. Adsorption kinetics, thermodynamics, and adsorption isotherms were used to evaluate the sorption process. XPS analysis was employed to predict the adsorption mechanism. All of the fundamental research from this study supported a more efficient, low-cost method for the separation of zirconium and hafnium.

## 2. Experimental

### 2.1 Materials and methods

Chemicals including methyl acrylate (MA), ethylenediamine (EDA), (3-aminopropyl) trimethoxysilane (APTES), phenylphosphonic dichloride (PS), tetraethyl orthosilicate (TEOS), cetyltrimethylammonium bromide (CTAB), silica gel (200–300 mesh), acetic acid and nitric acid were used as received from Aladdin. The stock solution was prepared by dissolving appropriate amounts of $ZrOCl_2 \cdot 8H_2O$ and $HfOCl_2 \cdot 8H_2O$ in HCl solution. All the chemicals mentioned above were analytical grade or better.

### 2.2 Preparation of phosphorous-functionalized PAMAM dendrimers supported on mesoporous silica

Approaches for synthesizing phosphorous-functionalized PAMAM grafted on mesoporous silica (PS-G1.0-MSNs) are given in Scheme 1. The synthetic detail process is as follows:

**2.2.1 Synthesis of mesoporous silica (MSNs).** Mesoporous silica (MSNs) was employed as the hard carrier in this study, and was prepared as previously reported.[35] Here, 2.0 g CTAB was suspended in 300 mL of distilled water and 0.56 g sodium hydroxide was added, and then the mixture was slowly heated to 80 °C. Next, 5.3 mL TEOS was added to the mixture drop by drop and stirred at 80 °C for 2 h. The crude product was filtered, washed with ultrapure water and methanol, respectively, and then dried naturally to obtain the pure MSNs carrier. The synthesized MSNs were rewashed with ethanol and water to get rid of the excess CTAB, then the product was dried in a vacuum drying oven for 6 h at 60 °C to obtain the pure product MSNs.

**2.2.2 Preparation of the APTES-modified G1.0 PAMAM dendrimer.** The APTES-modified G1.0 PAMAM dendrimer (G1.0-APTES) was prepared using a modified multistep process as previously reported.[36] Here, 10 mL APTES was dissolved in 30 mL ethanol and 8.6 g excess MA was added drop by drop, then stirred at 30 °C under a $N_2$ atmosphere for 24 h. The G0.5-APTES was obtained by filtration and washed with methanol. A sample of 11.8 g G0.5-ATTES and 4.8 g EDA was dissolved in 30 mL methanol, and then the mixture was refluxed at 30 °C under a $N_2$ atmosphere for 24 h. After filtration and washing with methanol, the product G1.0-APTES was obtained.

**2.2.3 Preparation of phenylphosphonic dichloride (PS) functionalized G1.0-APTES dendrimers (PS-G1.0-APTES).** The synthesis of PS-G1.0-APTES as the reported ref. 37, 5 mL of phenylphosphonic dichloride (PS), 30 mL dry ethanol, and 7.8 g G1.0-APTES were mixed in a 250 mL three-necked flask, and 1 mL of triethylamine was added dropwise and heated for 24 h under a nitrogen atmosphere. Then the mixture was filtered off, washed with ethanol and ultrapure water, then the product PS-G1.0-APTES was obtained after drying in a vacuum oven at 60 °C for 12 h.

**2.2.4 Preparation of PS-G1.0-APTES supported on MSNs (PS-G1.0-MSNs).** Here, 10 g MSNs and 2 g PS-G1.0-APTES were suspended in 35 mL of anhydrous DMF, and the suspension was refluxed for 12 h under a nitrogen atmosphere. After filtration, washing with deionized water and methanol, and drying under vacuum conditions, the PS-G1.0-APTES bound on MSNs (PS-G1.0-MSNs) was obtained.

### 2.3 Batch adsorption on Zr(IV) and Hf(IV)

Batch sorption studies were performed on PS-G1.0-MSNs; the effects of solution acidity (pH 0.5–3.0), contact time (10–120 min), initial metal ion concentration, as well as temperature (20–80 °C), were examined. In a typical test, 50 mg of the synthesized sorbent PS-G1.0-MSNs were suspended in 10 mL of Zr(IV) and Hf(IV) mixture solutions. The stock concentrations of Zr(IV) and Hf(IV) were $5 \times 10^{-3}$ mol $L^{-1}$ and $3 \times 10^{-4}$ mol $L^{-1}$ respectively, and the molar ratio of Zr(IV) and Hf(IV) was simulated as present in nature. The mixture solution was shaken at 25 °C from 20 to 120 min, then filtered and the concentration was determined by ICP-AES. The sorption amount $Q_e$ (mg $g^{-1}$), distribution ($D$), and separation coefficient ($\beta_{Hf/Zr}$) were determined using the following formulas:[38]
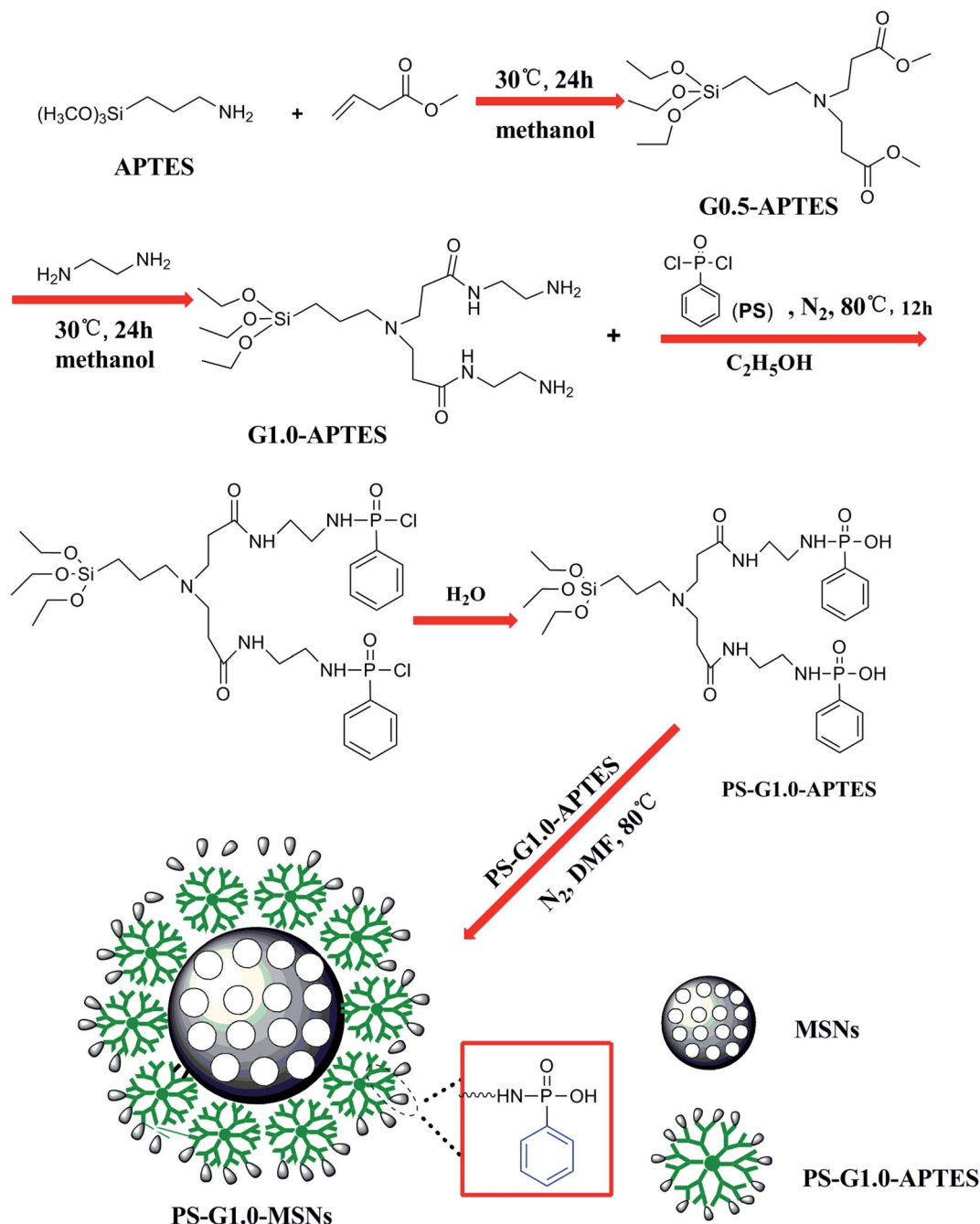
$$Q_e = \frac{(C_0 - C_e) \times V}{W} \quad (1)$$

$$D = \frac{C_0 - C_e}{C_0} \quad (2)$$

$$\beta_{Hf/Zr} = \frac{D_{Hf}}{D_{Zr}} \quad (3)$$

Here $C_0$ is the initial concentration of Zr(IV) or Hf(IV), and $C_e$ is the equilibrium residual metal ion concentration in solution (mg $L^{-1}$); $V$ is the volume of experimental solution (mL); $W$ is the weight of PS-G1.0-MSNs (g).

**Scheme 1 Synthesis of the PS-G1.0-MSNs sorbent**

Scheme 1  Synthesis of the PS-G1.0-MSNs sorbent.

## 2.4  Characterization

The FT-IR spectra were obtained by using a Nicolet AVATAR 360 spectrophotometer *via* the KBr pellet method; the resolution was 4 cm$^{-1}$, and the scan wavenumber was from 400 to 4000 cm$^{-1}$. XRD analysis was conducted at 40 kV and 10 mA with nickel-filtered Cu Kα radiation by using an XRD-600 instrument. TEM was conducted using a JEOL JEM-200CX transmission electron microscope operated at 200 kV. XPS was conducted using an AXIS Ultra DLD spectrometer. TGA investigation was carried out on a STA409PC with a 10 °C min$^{-1}$ rate of heat addition from 10 to 800 °C in a nitrogen atmosphere. BET testing was used to calculate the surface areas. The concentrations of Zr(IV) and Hf(IV) ions were determined by ICP-AES (Thermo Optima 8000D).

# 3.  Results and discussion

## 3.1  Characterization of PS-G1.0-MSNs

**3.1.1  FT-IR study.** FT-IR is a convenient method for analyzing the reaction process. The FT-IR spectra of the synthesized G1.0-APTES, PS-G1.0-APTES, MSNs, and PS-G1.0-APTES composites are shown in Fig. 1.

For G1.0-APTES (Fig. 1a), the bands at 2950 $cm^{-1}$ and 2850 $cm^{-1}$ were caused by the stretching vibration of C–H bands; the peak at 1740 $cm^{-1}$ corresponds to the –COO stretching vibration, which indicates the successful Michael addition of MA to the –$NH_2$ groups G0.5.[39] For the spectrum of PS-G1.0-APTES (Fig. 1b), the new bands at 1150 $cm^{-1}$ and 3400 $cm^{-1}$ were attributed to the P=O and O–H stretching vibration, respectively, which indicated the successful grafting of phenylphosphonic dichloride on the G1.0-APTES dendrimer.[40] In the spectrum of MSNs (Fig. 1c), the broad peak at around 3430 $cm^{-1}$ was ascribed to the O–H stretching vibration. The bands at 805 and 472 $cm^{-1}$ were related to the symmetric and bending vibrations of Si–O–Si in the network of MSNs, respectively.[41] A new peak at 1740 $cm^{-1}$ was caused by the C=O stretching vibration of PS-G1.0-MSNs (Fig. 1d) as compared with the pure MSNs. All the results confirmed that PS-G1.0-APTES was covalently grafted on the MSNs carrier successfully. Thus, the step-by-step synthesis of the phosphorous-functionalized G1.0 PAMAM dendrimer on the MSNs surface was monitored by FT-IR.

**3.1.2  Surface properties, SEM and TGA analysis of PS-G1.0-MSNs.** The adsorption–desorption isotherms of PS-G1.0-MSNs were obtained under $N_2$ atmosphere and are shown in Fig. 2. The calculated parameters such as surface area, pore volume, and pore diameter are listed in Table 1. The specific surface area of 256.87 $m^2$ $g^{-1}$, pore volume of 0.614 $cm^3$ $g^{-1}$, and average mesopore diameter of 11.02 nm for MSNs were examined by BET analysis. The recorded parameters of PS-G1.0-MSNs decreased as expected, which was caused by the modification
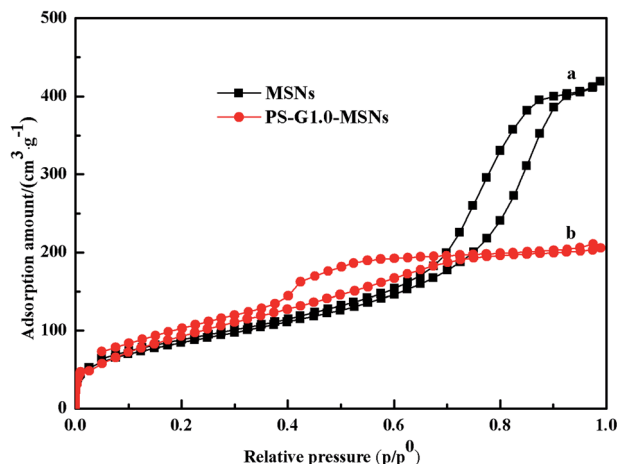


**Fig. 2**  $N_2$ adsorption–desorption isotherms of the synthesized MSNs (a) and PS-G1.0-MSNs (b) sorbents.

**Table 1**  Specific surface area of MSNs and PS-G1.0-MSNs

| Sorbents | Surface area ($m^2$ $g^{-1}$) | Pore diameter (nm) | Pore volume ($cm^3$ $g^{-1}$) |
| --- | --- | --- | --- |
| MSNs | 256.87 | 11.02 | 0.614 |
| PS-G1.0-MSNs | 181.61 | 3.317 | 0.22 |

of the inner pore surface. It is worth noting that PS-G1.0-MSNs sorbents have moderate and suitable parameters as can be seen in Table 1 for metal ion adsorption.

Thermal gravimetric analysis (TGA) of the synthesized PS-G1.0-MSNs sorbents as shown in Fig. 3 was conducted from 10–800 °C at 10 °C $min^{-1}$ under $N_2$ atmosphere. There were two stages of decomposition on the curve of the PS-G1.0-MSNs sorbent: the first weight loss from 75 to 300 °C was caused by the evaporation of the residual water, while the further weight loss from 300 °C was attributed to the decomposition of the PAMAM organic components. The weight loss of MSNs (a), PS-
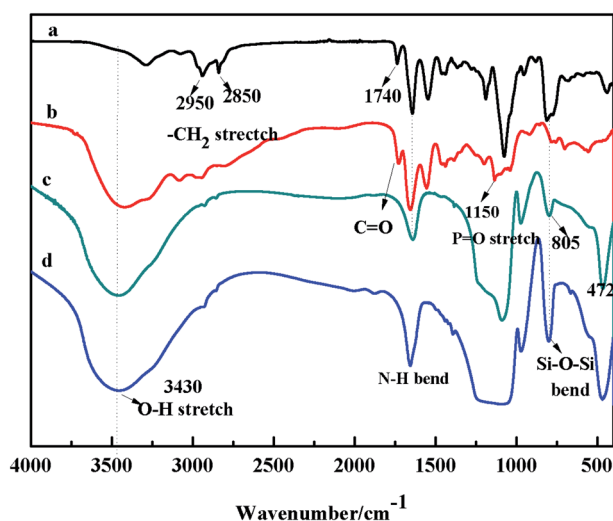


**Fig. 1**  FT-IR spectra of (a) G1.0-APTES, (b) PS-G1.0-APTES, (c) MSNs and (d) PS-G1.0-APTES.
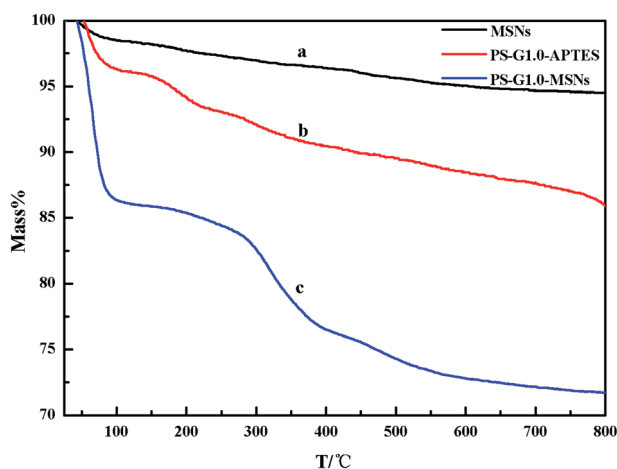


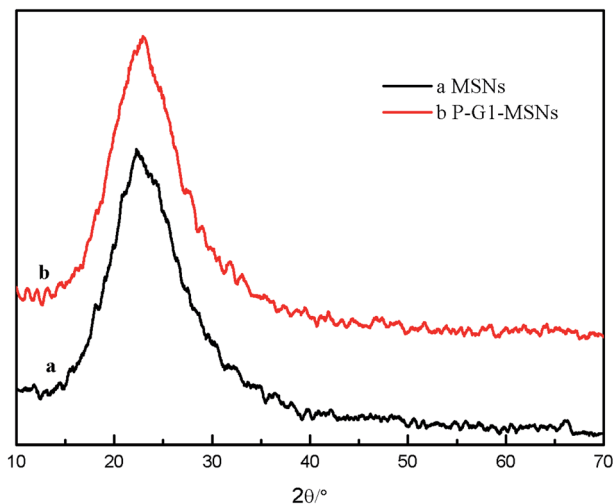**Fig. 3**  TGA curves of MSNs (a) PS-G1.0-APTES (b) and PS-G1.0-MSNs (c).

Fig. 4   XRD analysis of MSNs (a) and PS-G1.0-MSNs (b).



Fig. 6   The effects of acidity on the adsorption capacity $Q$ and separation factors $\beta_{Hf/Zr}$ of Zr(IV) and Hf(IV) on the PS-G1.0-MSNs sorbent.

G1.0-APTES (b), PS-G1.0-MSNs (c) was 5.43%, 13.68%, 28.35% as the temperature went up to 800 °C, respectively. By comparing the three curves, the increasing weight loss also confirmed that the G1.0 dendrimer was successfully loaded on the MSNs nanoparticles.

XRD patterns are shown in Fig. 4; the MSNs (Fig. 4a) and PS-G1.0-MSNs (Fig. 4b) had the same obvious characteristics of diffraction peaks with high intensity at $2\theta = 25°$, which indicated that the MSNs have relatively high crystal integrity as previously reported.[42] When MSNs were modified with PAMAM dendrimers, the position of the diffraction peak did not change, which demonstrated that the PAMAM was grafted on the MSNs surface through bonding with the silane coupling agent APTES, so the surface content of $SiO_2$ increased but the crystal structure of the MSNs was not destroyed after modification.

To confirm the formation of MSNs and PS-G1.0-MSNs, TEM images were taken as shown in Fig. 5. Fig. 5a and b clearly show the existence of mesoporous channels. When MSNs were incorporated with the PAMAM dendrimers, the nanoparticle shape did not change significantly, indicating that the MSNs can still keep their morphology and the mesoporous channels can still be found after functionalization.
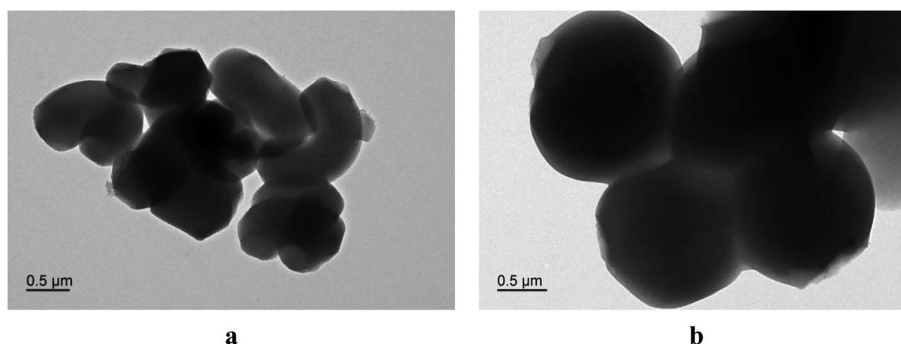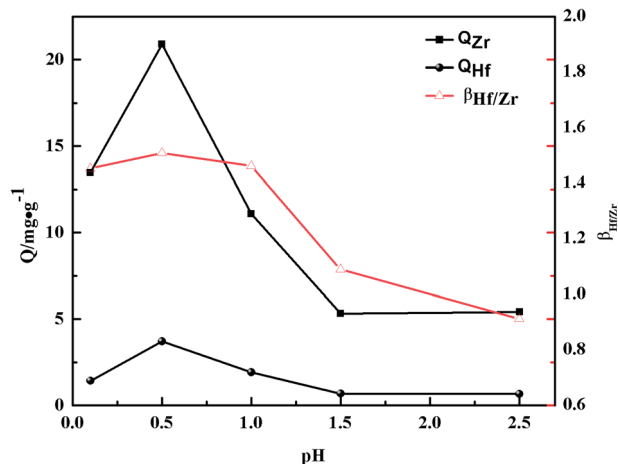
## 3.2   Zr(IV) and Hf(IV) adsorption performance of PS-G1.0-MSNs

### 3.2.1   The effects of acidity.
The effect of acidity on adsorption was examined by shaking 50 mg of dry sorbent with 10 mL stock solutions of Zr(IV) and Hf(IV) for 120 min in the pH range of 0.1–3.0 in case the Zr(IV) and Hf(IV) ions converted into insoluble species. The adsorption capacities of Zr(IV) and Hf(IV), and the separation coefficient ($\beta_{Zr/Hf}$) are presented in Fig. 6. The adsorption capacity of PS-G1.0-MSNs on Zr(IV) and Hf(IV) was greatly affected by the pH value; the adsorption amount increased sharply with the increasing pH value under 0.5. Conversely, when the solution pH > 0.5, the adsorption amount decreased as the pH value increased, and the maximum adsorption capacities were $Q_{Zr} = 20.9$ mg g$^{-1}$ and $Q_{Hf} = 3.7$ mg g$^{-1}$ at around pH 0.5, respectively.

The results might be caused by different species of Zr(IV) and Hf(IV) in different acidity.

In lower pH solution, the predominant form of Zr(IV) was Zr$^{4+}$; as the pH value increased, the hydrolysis species such as [Zr(OH)]$^{3+}$, [Zr(OH)$_2$]$^{2+}$, [Zr(OH)$_4$], [Zr(OH)$_5$]$^-$ dominated, whereas the main species was ZrO$^{2+}$ at higher pH (>3).[43,44] There were –NH and O=P–OH groups in the modified sorbent, which could form complexes with zirconium and hafnium. At lower



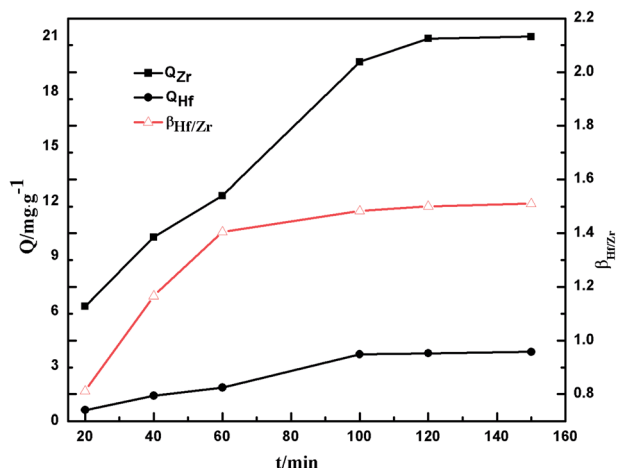Fig. 5   TEM analysis of MSNs (a) and PS-G1.0-MSNs (b).

Fig. 7 The effects of contact time on the adsorption capacity $Q$ and separation factors $\beta_{Zr/Hf}$ of Zr(IV) and Hf(IV) on PS-G1.0-MSNs.

pH, the N atom of –NH became protonated, and the phosphoric OH dissociated in the alkaline region, and thus led to the negative surface charge of the sorbent, which would explain the decreasing adsorption of Zr(IV) with increasing pH > 0.5. The adsorption trend affected by the pH of PS-G1.0-MSNs on Hf(IV) had a similar tendency to Zr(IV), which was induced by their similar chemical properties. Furthermore, the separation coefficient of $\beta_{Hf/Zr}$ showed a similar trend to the adsorption capacity and $\beta_{Hf/Zr} > 1$, which implied that the PS-G1.0-MSNs sorbent preferably extracted Hf(IV) in the mixture solution, so pH 0.5 was selected for subsequent adsorption research.

**3.2.2 Kinetics study.** To investigate the sorption mechanism, the contact time and adsorption kinetics were studied by the following process. Each feed solution (10 mL, pH 0.5) and 50 mg PS-G1.0-MSNs sorbent were shaken at 25 °C for the scheduled time (20–120 min) to analyze the residual concentrations of metal ions by ICP-AES, and the outcomes are presented in Fig. 7.

It was observed that the sorption of Zr(IV) and Hf(IV) was rapid in the first 60 min, then gradually reached equilibrium within 120 min, and the maximum equilibrium adsorption amounts were 20.9 mg g$^{-1}$ and 3.7 mg g$^{-1}$ for Zr(IV) and Hf(IV), respectively. Zr(IV) and Hf(IV) had similar adsorption trends on PS-G1.0-MSNs, and the separation factor of $\beta_{Hf/Zr}$ increased as time increased, which was up to 1.6 at 120 min; in other words, the synthesized sorbent of PS-G1.0-MSNs has preferential selectivity on hafnium. From the contacting study, the results showed that 120 min was sufficient to attain equilibrium, and so the later tests were performed within 120 min.
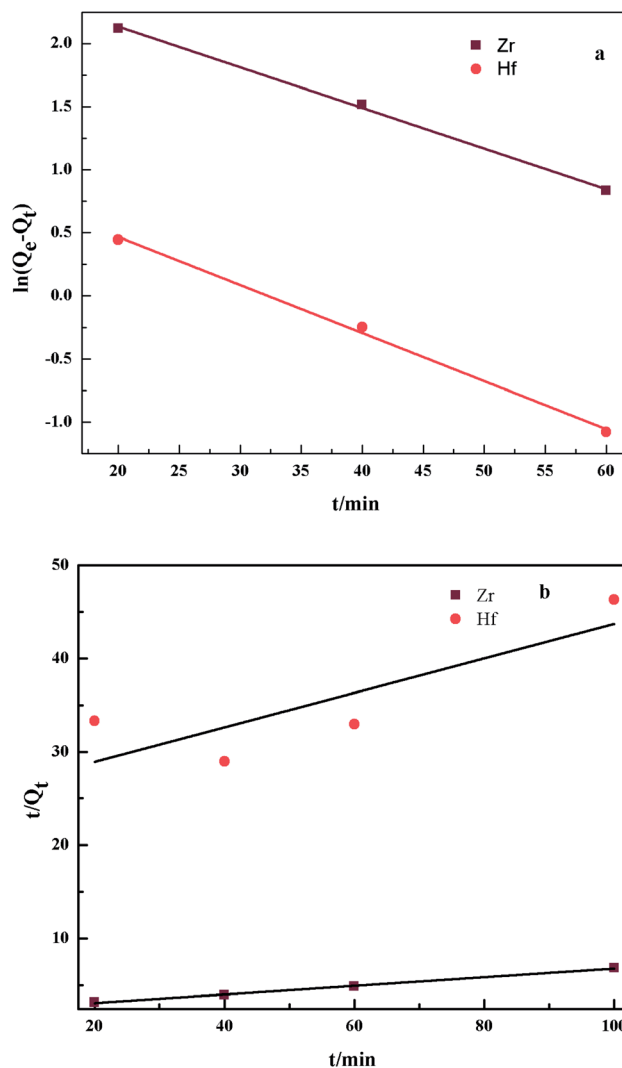


Fig. 8 The pseudo-first-order kinetics (a) and the pseudo-second-order kinetics (b) for the adsorption of Zr(IV) and Hf(IV) on PS-G1.0-MSNs sorbents.

There are generally three steps that can be employed to describe the adsorption process: the first one is the mass transfer of the liquid phase to the surface of the particle, the second is the diffusion inside the pores of the particle, and the third is surface adsorption.[45] To investigate the decisive adsorption rate parameters, two kinetic models, pseudo-first-order and pseudo-second-order, were employed in the experiment.[46] The mathematical expressions of the two models are listed in eqn (4) and (5), respectively:

Table 2  Calculated kinetic parameters of Zr(IV) and Hf(IV) adsorption on PS-G1.0-MSNs sorbents

| Metal ions | $Q_e$ exp/mg g$^{-1}$ | Pseudo-first-order model | | | Pseudo-second-order model | | |
|---|---|---|---|---|---|---|---|
| | | $K_1$/min$^{-1}$ | $Q_{e,cal}$/mg g$^{-1}$ | $R^2$ | $K_2$/mg g$^{-1}$ min$^{-1}$ | $Q_{e,cal}$/mg g$^{-1}$ | $R^2$ |
| Zr(IV) | 14.62 | 0.043 | 105.86 | 0.998 | $1.610 \times 10^{-3}$ | 152.56 | 0.997 |
| Hf(IV) | 2.16 | 0.044 | 142.76 | 0.998 | $7.258 \times 10^{-3}$ | 202.2 | 0.703 |

Fig. 9 The effects of temperature on the adsorption of Zr(IV) and Hf(IV) on the PS-G1.0-MSNs sorbent.

Table 3 Thermodynamic parameters for the adsorption of Zr(IV) and Hf(IV) on PS-G1.0-MSNs sorbents

| | $T$ (K) | 293.15 | 303.15 | 323.15 | 333.15 |
|---|---|---|---|---|---|
| Zr | $\Delta S$ (J mol$^{-1}$ K$^{-1}$) | 121.55 | 121.55 | 121.55 | 121.55 |
| | $\Delta H$ (kJ mol$^{-1}$) | 15.77 | 15.77 | 15.77 | 15.77 |
| | $\Delta G$ (kJ mol$^{-1}$) | −19.86 | −21.08 | −23.51 | −24.72 |
| | $T\Delta S$ (kJ mol$^{-1}$) | 35.63 | 36.85 | 39.28 | 40.49 |
| Hf | $\Delta S$ (J mol$^{-1}$ K$^{-1}$) | 112.57 | 112.57 | 112.57 | 112.57 |
| | $\Delta H$ (kJ mol$^{-1}$) | 18.18 | 18.18 | 18.18 | 18.18 |
| | $\Delta G$ (kJ mol$^{-1}$) | −14.82 | −15.95 | −18.2 | −19.32 |
| | $T\Delta S$ (J mol$^{-1}$) | 33.00 | 34.12 | 36.38 | 37.50 |

that the decisive adsorption on Zr(IV) and Hf(IV) is the rate-determining step.

**3.2.3 The effect of thermodynamics.** The impacts of temperature on Zr(IV) and Hf(IV) adsorption were investigated from 293 K to 343 K and the outcomes are presented in Fig. 9. The adsorption capacities increased as the temperature increased from 293 to 323 K and then decreased after 323 K. The results indicate that 323 K was the optimal temperature for Zr(IV) and Hf(IV) adsorption, and the maximum adsorption capacity for Zr(IV) and Hf(IV) was 23.68 and 4.26 mg g$^{-1}$, respectively at the optimal conditions. Furthermore, the separation factor $\beta_{Hf/Zr}$ also increased as temperature increased from 293 to 323 K and reached to 1.93, which may be induced by the hindrance and special cavity of the PS-G1.0-MSNs formed in the preparation process by loading the G1.0 PAMAM dendrimer on MSNs. The cavity of the adsorbent gets smaller or larger, depending on the different extension levels of the dendrimers as the temperature changes, and the interactions between the metal ions and sorbent also become stronger or weaker accordingly.[47]

To investigate whether the adsorption was a physical or chemical process, the thermodynamic model was employed according to the following equation:[48,49]

$$\ln\left(\frac{Q_e}{C_e}\right) = \frac{\Delta S}{R} - \frac{\Delta H}{R} \times \frac{1}{T} \qquad (6)$$

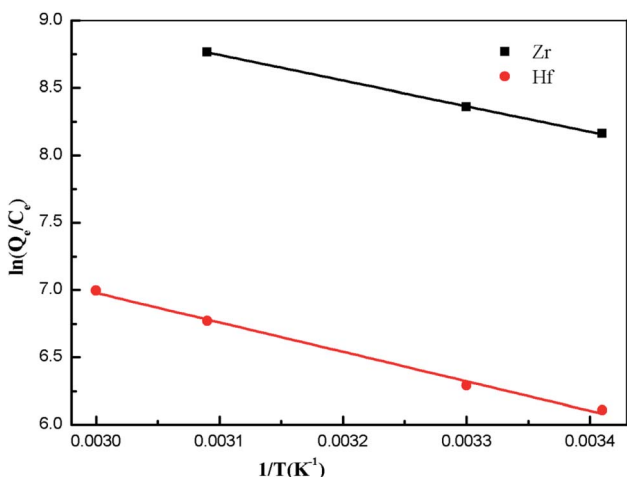$$\Delta G = \Delta H - T\Delta S \qquad (7)$$

$Q_e$, and $C_e$ (mg L$^{-1}$) are the adsorption capacity at equilibrium for Zr(IV) and Hf(IV), respectively, $R$ is 8.315 J K$^{-1}$ mol$^{-1}$, and $T$ is the absolute temperature; $\Delta S$ is entropy, $\Delta H$ is enthalpy change and $\Delta G$ is the change of Gibbs free energy. The values of $\Delta S$ and $\Delta H$ can be calculated by plotting $\ln(Q_e/C_e)$ versus $1/T$ from 283 K to 323 K. The plotted figures are listed in Fig. 10 and the calculated parameters are all shown in Table 3.

From 283 K to 323 K, the $\Delta G$ values were negative, indicating that the sorption was spontaneous and the feasibility of the adsorption process was also verified. $\Delta H$ and $\Delta S$ were positive, which implied an endothermic nature and increasing randomness at the solid–liquid interface during the Zr(IV)/Hf(IV) adsorption on PS-G1.0-MSNs. The value of $\Delta H$ was close to the general reaction enthalpy and the value of $\Delta S$ was also large.[50] The independence indicated that Zr(IV)/Hf(IV) adsorption on PS-G1.0-MSNs was mainly chemical adsorption.

$$-\ln(Q_e - Q_t) = K_1 \times t - \ln Q_e \qquad (4)$$

$$\frac{t}{Q_t} = \frac{1}{K_2 \times Q_e^2} + \frac{t}{Q_e} \qquad (5)$$

Here $Q_t$ is the adsorption amount at any given moment; $Q_e$ is the equilibrium adsorption capacity; $K_1$ is the rate constant of adsorption. Two lines were acquired by plotting $-\ln(Q_e - Q_t)$ against $t$ (Fig. 6a) according to eqn (4). The calculated parameters such as $K_1$, $K_2$, $Q_e$, and $R^2$ were generated and shown in Table 2 and Fig. 8 through batch studies by the two models.

The adsorption rate constant read from the line was 0.043 min$^{-1}$ and 0.044 min$^{-1}$ for Zr(IV) and Hf(IV), respectively. The correlation coefficient $R^2$ was 0.998for both Zr(IV) and Hf(IV), obtained by the linear fitting of the first model, whereas $R^2$ obtained by the second model was 0.997 and 0703 for Zr(IV) and Hf(IV), respectively. As such, the adsorption of PS-G1.0-MSNs on Zr(IV) and Hf(IV) could be better expressed by the pseudo-first-order kinetic model because of their higher $R^2$. This implies



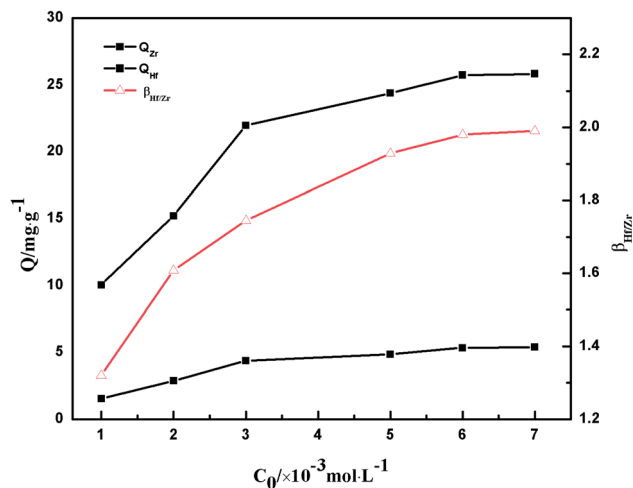Fig. 10 The thermodynamics data analysis by fitting $\ln(Q_e/C_e)$ versus $1/T$ from 283 K to 333 K.

**Fig. 11** The effects of concentration on the adsorption capacity $Q$ and separation factor $\beta_{Hf/Zr}$ of Zr(IV) and Hf(IV) on PS-G1.0-MSNs.

**3.2.4 Adsorption isotherms.** Adsorption isotherms were obtained by changing the initial Zr(IV) and Hf(IV) total concentrations in the range of $0.5$–$7.0 \times 10^{-3}$ mol L$^{-1}$ at pH 0.5 (Fig. 11). The adsorption amount of PS-G1.0-MSNs sorbent on Zr(IV) and Hf(IV) ($Q_{Zr}$ and $Q_{Hf}$) increased with the increasing concentration of $C_{e,Zr+Hf}$. When the concentration was up to $5.0 \times 10^{-3}$ mol L$^{-1}$, the rate of adsorption capacity increased slowly, and the maximum adsorption amounts were 25.74 and 5.36 mg g$^{-1}$ for Zr(IV) and Hf(IV) at the concentration of $6.0 \times 10^{-3}$ mol L$^{-1}$, respectively. Moreover, the separation factor $\beta_{Hf/Zr}$ had a similar trend to the adsorption capacity change with the concentration and it was up to the maximum of 2.0, which was higher than previously reported for crown ether supported on silica gel.[51]

The relationship between ions adsorbed on the PS-G1.0-MSNs sorbents and the sorption equilibrium could be described by the adsorption isotherm. Here, the Langmuir and the Freundlich equations[52] (eqn (8) and (9)) were employed, and the plotted results are given in Fig. 12 and Table 4.

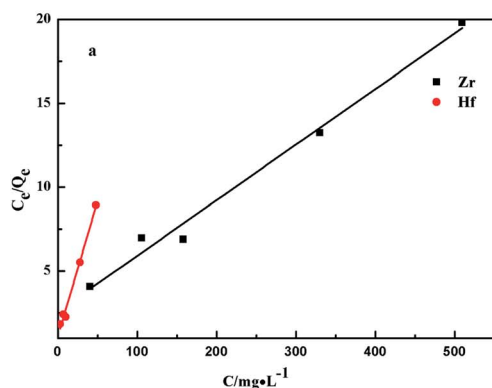$$\text{Langmuir}: \quad \frac{C_e}{Q_e} = \frac{1}{K_L \times Q_{max}} + \frac{C_e}{Q_{max}} \tag{8}$$

**Table 4** Fitting parameters of the Langmuir and Freundlich models at 25 °C

| Ions | Langmuir | | | Freundlich | | |
|---|---|---|---|---|---|---|
| | $Q_m$ (mg g$^{-1}$) | $K_L$ (L mg$^{-1}$) | $R_L^2$ | $K_F$ | $n$ | $R_F^2$ |
| Zr(IV) | 30.18 | 1.36 | 0.99 | 2.42 | 2.57 | 0.98 |
| Hf(IV) | 6.21 | 2.99 | 0.99 | 1.08 | 2.30 | 0.94 |

$$\text{Freundlich}: \quad \ln Q_e = \ln K_F + \frac{1}{n} \times \ln C_e \tag{9}$$

Here $Q_e$ (mg g$^{-1}$) and $Q_{max}$ are the experimental and the calculated maximum adsorption capacity, respectively. $C_e$ (mg L$^{-1}$) is the experimental concentration of Zr(IV) and Hf(IV) at equilibrium. $K_L$ (L mg$^{-1}$) is the empirical parameter obtained from the intercept of the linear fitting result, $K_F$ is the binding energy constant and $1/n$ is the heterogeneity factor.

As seen from Fig. 12 and Table 4, a straight line ($R^2 > 0.99$) was obtained by plotting $C_e/Q_e$ against $C_e$. The results indicated that the Langmuir adsorption isotherm agreed well with Zr(IV) and Hf(IV) sorption on PS-G1.0-MSNs. The calculated maximum adsorption capacity ($Q_{max}$) was 30.18 mg g$^{-1}$ and 6.21 mg g$^{-1}$ on Zr(IV) and Hf(IV), respectively. The calculated Langmuir constant $K_L$ for Zr(IV) and Hf(IV) was 1.36 and 2.99 L mg$^{-1}$, respectively. As is well known, the Langmuir isotherm is used to describe homogeneous sorption, and the smaller the $K_L$, the weaker the adsorption. It could, therefore, be concluded that the adsorption of PS-G1-MSNs towards Hf(IV) was stronger than that of the Zr(IV).

**3.2.5 XPS analysis.** To reveal the adsorption mechanism, XPS was used to analyze the components of the PS-G1.0-MSNs particles before and after adsorption.

Fig. 13 shows the survey spectra of the total scan of PS-G1.0-MSNs (a) before and after adsorption, and signals of the C 1s, N 1s, O 1s, P 2p, Zr 3d, and Hf 4f were recorded. From Fig. 13a, we can see that the signal of Zr 3d and the Hf 4f with weak intensity appeared at 183.4 eV and 14.5 eV after adsorption, respectively, which confirmed the sorption of Zr(IV) and Hf(IV) on PS-G1.0-MSNs after equilibration in the mixture solution. The peak at
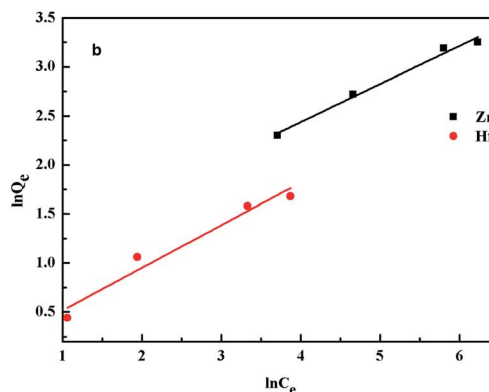


**Fig. 12** Adsorption isotherms of Zr(IV) and Hf(IV) on the PS-G1.0-MSNs sorbent by the Langmuir (a) and Freundlich (b) models.
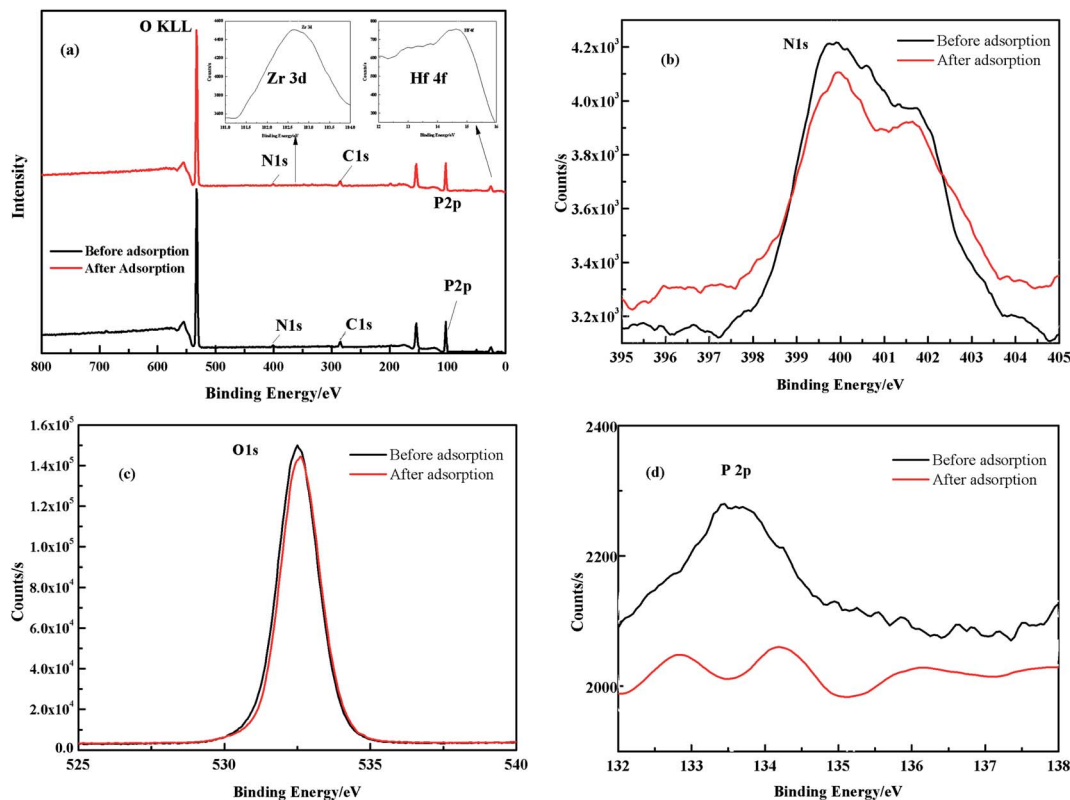
**Fig. 13** XPS survey spectra of PS-G1.0-MSNs before and after the adsorption of Zr(ɪv) and Hf(ɪv), where (a) is the total survey scan of PS-G1.0-MSNs, (b) is the scan of N 1s, (c) is the scan of O 1s and (d) is the scan of P 2p.

532.5 eV was attributed to O 1s of the C=O group, and the peak of N 1s around 399 eV was attributed to –NH– or –NH⁺•– functional groups of PS-G1.0-MSNs.[53] The peaks at 399.7 eV of the N 1s area after Zr(ɪv)/Hf(ɪv) sorption showed a corresponding decrease and shifted to 399.9 eV as indicated in Fig. 13b. It was also noted that peaks at 532.5 eV of O 1s after Zr(ɪv)/Hf(ɪv) sorption also demonstrated a corresponding decrease and certain shift (Fig. 13c). Furthermore, the peak at 133.4 eV of P 2p

split into two peaks and showed a corresponding decrease after adsorption as seen from Fig. 13d. All the results demonstrated that the adsorption of PS-G1.0-MSNs on Zr(ɪv) and Hf(ɪv) was probably introduced by the chemical coordination of N, O, P atoms of –CONH₂, –NH₂ and –PO₃ groups with Zr(ɪv) and Hf(ɪv). A deduced binding mechanism of PS-G1.0-MSNs on Zr(ɪv) and Hf(ɪv) was proposed and illustrated in Fig. 14.
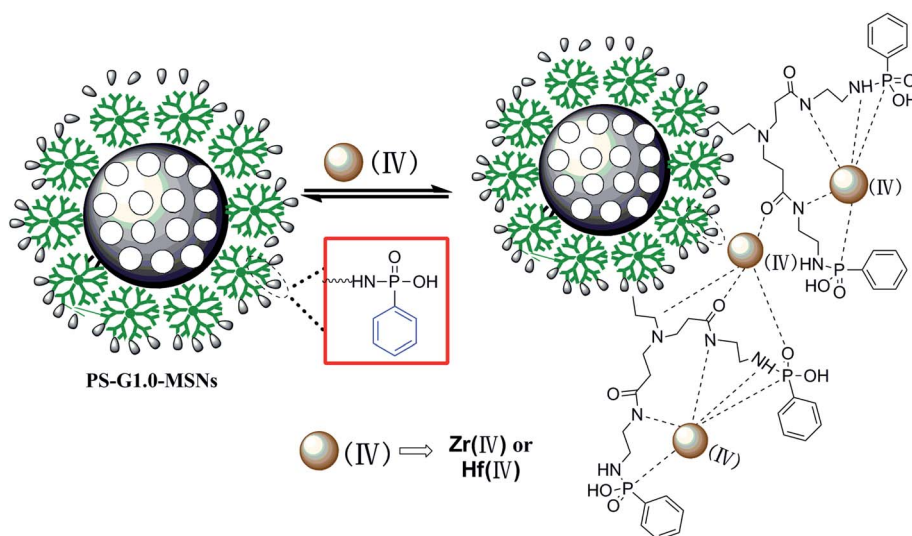


**Fig. 14** Proposed chelating mechanism of the PS-G1.0-MSNs sorbent with Zr(ɪv) and Hf(ɪv).

# 4. Conclusion

In summary, a new mesoporous silica-bound phosphorous-functionalized G1.0 PAMAM dendrimer (PS-G1.0-MSNs) with excellent adsorption properties on Zr(IV) and Hf(IV) was prepared. Batch sorption experiments showed that the maximum adsorption amounts were 25.7 mg g$^{-1}$ and 5.36 mg g$^{-1}$ on Zr(IV) and Hf(IV), respectively, under pH 0.5 in 120 min with the total concentration of $6.0 \times 10^{-3}$ mol L$^{-1}$. Furthermore, the prepared sorbent had preferential selectivity on hafnium and the maximum separation factor was up to $\beta_{Hf/Zr} = 2.0$ under the optimal conditions. Kinetics data indicated that the sorption on Zr(IV) and Hf(IV) followed the pseudo-first-order model with a rate-determining step. Thermodynamics studies indicated that the sorption of Zr(IV) and Hf(IV) on PS-G1.0-MSNs was spontaneous from 283 to 323 K, whereas the negative $\Delta H$ and small $\Delta S$ indicated an exothermic Zr(IV)/Hf(IV) sorption at a higher temperature from 313 to 333 K. The Langmuir constant $K_L$ was 1.36 and 2.99 L mg$^{-1}$ for Zr(IV) and Hf(IV), respectively. The smaller the $K_L$ was, the weaker the adsorption. The results indicated that the sorption ability of P-G1-MSNs on Hf(IV) was stronger as compared to Zr(IV). Furthermore, XPS analysis revealed that the adsorption of Zr(IV) and Hf(IV) was probably induced by the chemical coordination of Zr(IV) and Hf(IV) ions with N, O, P atoms of –CONH$_2$, –NH$_2$ and –PO$_3$ groups. All the results demonstrated that the PS-G1.0-MSNs might potentially be an excellent sorbent that could preferentially extract hafnium from zirconium-rich solutions.

## Conflicts of interest

All of the authors declare that they have no known competing financial interests or personal relationships that could have appeared to influence the work reported in this paper.

## References

1 L. Xu, Y. Xiao, A. van Sandwijk, Q. Xu, et al., Production of nuclear grade zirconium: a review, J. Nucl. Mater., 2015, 466, 21–28.

2 A. Das, K. R. S. Chandrakumar, B. Paul, S. M. Chopade, et al., Enhanced adsorption and separation of zirconium and hafnium under mild conditions by phosphoric acid based ligand functionalized silica gels: insights from experimental and theoretical investigations, Sep. Purif. Technol., 2020, 239, 116518.

3 R. K. Biswas and M. A. Hayat, Solvent extraction of zirconium (IV) from chloride media by D2EHPA in kerosene, Hydrometallurgy, 2002, 63, 149–158.

4 L. Y. Wang, H. Y. Lee and M. S. Lee, Solvent extraction separation of Zr and Hf from nitric acid solutions by PC 88A and its mixture with other extractants, Met. Mater. Int., 2015, 21, 166–172.

5 S. Chen, Z. F. Zhang, S. T. Kuang, et al., Separation of zirconium from hafnium in sulfate medium using solvent extraction with a new reagent BEAP, Hydrometallurgy, 2017, 169, 607–611.

6 B. R. Keddy, J. R. Kumar, K. P. Raja, et al., Solvent extraction of Hf (IV) from acidic chloride solutions using Cyanex 302, Miner. Eng., 2004, 17, 939–942.

7 B. C. Bhatta, N. Panda and S. Mishra, Extraction of Zr (IV) from hydrochloric acid with tri-octyl amine and Cyanex 921 in kerosene, Int. J. Miner., Metall. Mater., 2013, 20, 823–828.

8 M. Taghizadeh, M. Ghanadi and E. Zolfonun, Separation of zirconium and hafnium by solvent extraction using mixture of TBP and Cyanex 923, J. Nucl. Mater., 2011, 412, 334–337.

9 L. Y. Wang, H. Y. Lee and M. S. Lee, Solvent extraction of zirconium and hafnium from hydrochloric acid solutions using acidic Organophosphorus extractants and their mixtures with TOPO, Mater. Trans., 2013, 54, 1460–1466.

10 Y. L. Wang and M. S. Lee, Separation of zirconium and hafnium from nitric acid solutions with LIX 63, PC 88A and their mixture by solvent extraction, Hydrometallurgy, 2014, 150, 153–160.

11 Z. G. Xu, Y. K. Wu, J. D. Zhang, et al., Equilibrium and kinetic data of adsorption and separation for zirconium and hafnium onto MIBK extraction resin, Trans. Nonferrous Met. Soc. China, 2010, 20, 1527–1533.

12 L. Xu, Y. Xiao, A. Sandwijk, et al., Production of nuclear grade zirconium: a review, J. Nucl. Mater., 2015, 466, 21–28.

13 J. S. Liu, H. Chen and Z. L. Guo, Extraction and separation of In(III), Ga(III) and Zn(II) from sulfate solution using extraction resin, Hydrometallurgy, 2006, 82, 137–143.

14 X. B. Yin, Y. Z. Wei and J. H. Zu, Adsorption behavior of Zr(IV) and Hf(IV) on a silica-based macroporous TODGA adsorbent, Nucl. Sci. Tech., 2013, 24, 1–7.

15 W. Qin, S. M. Xu, G. Xu, Q. Xie and Z. H. Xu, Preparation of silica gel modified crown ether and its adsorption properties on zirconium and hafnium, Chem. Eng. J., 2013, 225, 528–534.

16 J. S. Liu, H. Chen and Z. L. Guo, Extraction and separation of In (III), Ga(III) and Zn(II) from sulfate solution using extraction resin, Hydrometallurgy, 2006, 82, 137–143.

17 Y. Z. Zhou, L. P. Luan, B. T. Tang, Y. Z. Niu, et al., Fabrication of Schiff base decorated PAMAM dendrimer/magnetic Fe$_3$O$_4$ for selective removal of aqueous Hg(II), Chem. Eng. J., 2020, 398, 125651.

18 Y. Niu, R. Qu, C. Sun, C. Wang, H. Chen, C. Ji, Y. Zhang, X. Shao and F. Bu, Adsorption of Pb(II) from aqueous solution by silica-gel supported hyperbranched polyamidoamine dendrimers, J. Hazard. Mater., 2013, 244–245, 276–286.

19 X. Z. Wu, L. L. Luo, Z. Y. Chen and K. L. Liang, Syntheses, characterization and adsorption properties for Pb$^{2+}$ of silica-gel functionalized by dendrimer-like polyamidoamine and 5-sulfosalicylic acid, *Appl. Surf. Sci.*, 2016, **364**, 86–95.

20 M. S. Diallo, S. Christie, P. Swaminathan, J. H. Johnson Jr and W. A. Goddard, Dendrimer enhanced ultrafiltration.1. Recovery of Cu(II) from aqueous solutions using PAMAM dendrimers with ethylene diamine core and terminal NH$_2$ groups, *Environ. Sci. Technol.*, 2005, **39**, 1366–1377.

21 P. Ilaiyaraja, A. K. Singha Deb, K. Sivasubramanian, D. Ponraju, *et al.*, Adsorption of uranium from aqueous solution by PAMAM dendron functionalized styrene divinylbenzene, *J. Hazard. Mater.*, 2013, **250**, 155–166.

22 Y. Z. Niu, R. Qu, C. Sun, C. Wang, H. Chen, C. Ji, Y. Zhang, X. Shao and F. Bu, Adsorption of Pb(II) from aqueous solution by silica-gel supported hyperbranched polyamidoamine dendrimers, *J. Hazard. Mater.*, 2013, **244–245**, 276–286.

23 X. Z. Wu, P. Liu, Q. S. Pu, Q. Y. Sun and Z. X. Su, Preparation of dendrimer-like polyamidoamine immobilized silica gel and its application to online preconcentration and separation palladium prior to FAAS determination, *Talanta*, 2004, **62**, 918–923.

24 Y. Niu, R. Qu, H. Chen, L. Mu, X. Liu, T. Wang, Y. Zhang and C. Sun, Synthesis of silica gel supported salicylaldehyde modified PAMAM dendrimers for the effective removal of Hg(II) from aqueous solution, *J. Hazard. Mater.*, 2014, **278**, 267–278.

25 Y. Z. Niu, J. Y. Yang, R. J. Qu and Y. H. Gao, Synthesis of Silica-Gel-Supported Sulfur-Capped PAMAM Dendrimers for Efficient Hg(II) Adsorption: Experimental and DFT Study, *Ind. Eng. Chem. Res.*, 2016, **55**, 3679–3688.

26 X. T. Song, Y. Z. Niu, Z. M. Qiu, Z. X. Zhang, Y. Z. Zhou, J. J. Zhao and H. Chen, Adsorption of Hg(II) and Ag(I) from fuel ethanol by silica gel supported sulfur-containing PAMAM dendrimers: kinetics, equilibrium and thermodynamics, *Fuel*, 2017, **206**, 80–88.

27 M. A. Barakat, M. H. Ramadan, M. A. Alghamdi, S. S. Algarny, H. L. Woodcock and J. N. Kuhn, Remediation of Cu(II), Ni(II), and Cr(III) ions from simulated wastewater by dendrimer/titania composites, *J. Environ. Manage.*, 2013, **117**, 50–57.

28 R. J. Qu, C. M. Sun, C. N. Ji, C. H. Wang and H. Chen, Preparation and metal-binding behavior of chitosan functionalized by ester- and amino-terminated hyper-branched polyamidoamine polymers, *Carbohydr. Res.*, 2008, **343**, 267–273.

29 F. Zhang, B. Wang, S. F. He and R. L. Man, Preparation of graphene-oxide/polyamidoamine dendrimers and their adsorption properties toward some heavy metal ions, *J. Chem. Eng. Data*, 2014, **59**, 1719–1726.

30 B. Hayati, A. Maleki, F. Najafi, H. Daraei, F. Gharibi and G. Mckay, Synthesis and characterization of PAMAM/CNT nanocomposite as a super capacity adsorbent for heavy metal (Ni$^{2+}$, Zn$^{2+}$, As$^{3+}$, Co$^{2+}$) removal from wastewater, *J. Mol. Liq.*, 2016, **224**, 1032–1040.

31 B. Hayati, A. Maleki, F. Najafi, H. Daraei, F. Gharibi and G. Mckay, Super high removal capacities of heavy metals (Pb$^{2+}$ and Cu$^{2+}$) using CNT dendrimer, *J. Hazard. Mater.*, 2017, **336**, 146–157.

32 X. Wu, L. Luo, Z. Chen and K. Liang, Syntheses, characterization and adsorption properties for Pb$^{2+}$ of silica-gel functionalized by dendrimer-like polyamidoamine and 5-sulfosalicylic acid, *Appl. Surf. Sci.*, 2016, **364**, 86–95.

33 X. Song, Y. Niu, P. Zhang, C. Zhang, *et al.*, Removal of Co(II) from fuel ethanol by silica-gel supported PAMAM dendrimers: combined experimental and theoretical study, *Fuel*, 2017, **199**, 91–101.

34 Y. R. Lee, S. Q. Zhang, K. W. S. Yu, J. B. Choi, *et al.*, Poly(amidoamine) dendrimer immobilized on mesoporous silica foam (MSF) and fibrous nano-silica KCC-1 for Gd$^{3+}$ adsorption in water, *Chem. Eng. J.*, 2019, **378**, 122–133.

35 X. B. Xu, S. Y. Lu, C. M. Gao, X. G. Wang, *et al.*, Facile preparation of pH-sensitive and self-fluorescent mesoporous silica nanoparticles modified with PAMAM dendrimers for label-free imaging and drug delivery, *Chem. Eng. J.*, 2015, **266**, 171–178.

36 R. Khodadust, G. Unsoy, S. Yalcın, G. Gunduz and U. Gunduz, PAMAM dendrimer-coated iron oxide nanoparticles: synthesis and characterization of different generations, *J. Nanoparticle Res.*, 2013, **15**, 1–13.

37 Q. Cao, Y. C. Liu, C. Z. Wang and J. S. Cheng, Phosphorus-modified poly(styrene-co-divinylbenzene)-PAMAM chelating resin for the adsorption of uranium(VI) in aqueous, *J. Hazard. Mater.*, 2013, **263**, 311–321.

38 E. Mohamed and S. M. Mohammed, Selective solid phase extraction and preconcentration of iron (III) based on silica gel chemically immobilized purpurogallin, *Anal. Chim. Acta*, 2001, **450**, 239–246.

39 Y. Z. Niu, R. J. Qu, H. Chen, L. Mu, *et al.*, Synthesis of silica gel supported salicylaldehyde modified dendrimers for the effective removal of Hg (II) from aqueous solution, *J. Hazard. Mater.*, 2014, **278**, 267–278.

40 Q. Cao, Y. C. Liu, C. Z. Wang and J. S. Cheng, Phosphorus modified poly(styrene-co-divinylbenzene)-chelating resin for the adsorption of uranium (VI) in aqueous, *J. Hazard. Mater.*, 2013, **263**, 311–321.

41 Y. Tian, P. Yin, R. J. Qu, C. H. Wang, H. G. Zheng and Z. X. Yu, Removal of transition metal ions from aqueous solutions by adsorption using a novel hybrid material silica gel chemically modified by triethylenetetraminomethylenephosphonic acid, *Chem. Eng. J.*, 2010, **162**, 573–579.

42 D. Lu, J. Lei, Z. Tian, L. Wang, *et al.*, Cu$^{2+}$ fluorescent sensor based on mesoporous silica nanosphere, *Dyes Pigm.*, 2012, **94**, 239–246.

43 A. W. Zhang, Y. Wei and M. Kumagai, Properties and mechanism of molybdenum and zirconium adsorption by a macroporous silica-based extraction resin in the MAREC process, *Solvent Extr. Ion Exch.*, 2003, **21**, 591–611.

44 S. Milonjic, M. Boskovic and T. Ceranic, Adsorption of uranium (VI) and zirconium (IV) from acid solution on silica gel, *Sep. Sci. Technol.*, 1992, **27**, 1643–1653.

45 B. C. Pan, Y. Xiong, Q. Su, A. M. Li, J. L. Chen and Q. X. Zhang, Role of amination of a polymeric adsorbent on phenol adsorption from aqueous solution, *Chemosphere*, 2003, **51**, 953–962.

46 V. C. Srivastava, I. D. Mall and I. M. Mishra, Adsorption thermodynamics and isosteric heat of adsorption of toxic metal ions onto bagasse fly ash (BFA) and rice husk ash (RHA), *Chem. Eng. J.*, 2007, **132**, 267–268.

47 W. Qin, G. Y. Qian, H. B. Tao, J. W. Wang, *et al.*, Adsorption of Hg(II) ions by PAMAM dendrimers modified attapulgite composites, *React. Funct. Polym.*, 2019, **136**, 75–85.

48 H. C. Ge, T. T. Hua and X. D. Chen, Selective sorption of lead on grafted and crosslinked chitosan nanoparticles prepared by using Pb$^{2+}$ as template, *J. Hazard. Mater.*, 2016, **308**, 225–232.

49 Z. X. Wang and H. C. Ge, Sorption of chromium (VI) from aqueous solution using a novel chitosan biguanidine, *J. Dispers. Sci. Technol.*, 2015, **36**, 1106–1114.

50 H. C. Ge and Z. W. Ma, Microwave preparation of triethylenetetramine modified grapheme oxide/chitosan composite for adsorption of Cr(VI), *Carbohydr. Polym.*, 2015, **131**, 280–287.

51 W. Qin, S. M. Xu, G. Xu, Q. Xie and Z. H. Xu, Preparation of silica gel modified crown ether and its adsorption properties on zirconium and hafnium, *Chem. Eng. J.*, 2013, **225**, 528–534.

52 S. P. Ramnani and S. Sabharwal, Adsorption behavior of Cr(VI) onto radiation crosslinked chitosan and its possible application for the treatment of wastewater containing Cr(VI), *React. Funct. Polym.*, 2006, **66**, 902–1002.

53 F. Gode and E. Pehlivan, Removal of chromium (III) from aqueous solutions using Lewatit S 100: the effect of pH, time, metal concentration and temperature, *J. Hazard. Mater.*, 2006, **136**, 330–337.